# Cycle-Aware Aging Cost Modeling of BESS via Dual Virtual Energy Distribution

Jiaxiong Xiang, *Student Member, IEEE*, Ming Zhou, *Senior Member, IEEE*,
Zhaoyuan Wu, *Member, IEEE*, Zhi Zhang, *Member, IEEE*

***Abstract*—Battery energy storage systems (BESS) are vital components of renewable-dominated power systems, but their operation is limited by battery aging. Aging mainly occurs during charge–discharge cycles, and conventional cycle identification using rainflow counting can only analyze SoC trajectories retrospectively. However, there is still a lack of analytical and accurate cycle cost models for optimization problems where SoC is a decision variable. To address this issue, this paper firstly models the BESS as a set of virtual slots, each assigned with a distinct marginal cycle increment. The dual energy distribution state is introduced to represent the marginal cycle-aging effects of charging and discharging processes. This method restores the Markov property of cycle aging and eliminates the dependence on historical paths and simulation. Based on this concept, a linear aging cost model with dual energy distributions is developed and seamlessly embedded into optimization frameworks such as BESS arbitrage or power system operation. Case studies show that the proposed model increases average arbitrage profit by 17.8% compared with traditional models. While conventional methods result in cost estimation errors of up to 44%, the proposed model achieves near-zero aging cost estimation error.When integrated into system scheduling, the model further reduces operating costs.**

***Index Terms*—Battery energy storage, Cycle aging cost Dual energy distribution, Markov property restoration.**

## I. Introduction

By the end of 2024, China's new energy storage capacity reached 73.76 GW/168 GWh, of which battery energy storage systems (BESS) accounted for over 90%. Despite this growth, BESS profitability remains limited by battery aging and replacement costs. As battery aging depends on complex charge–discharge cycling behavior, its operating cost is difficult to characterize. Therefore, developing a mathematical model that accurately represents the cycle-based aging cost of BESS for optimized operation is crucial to improving its operational and economic performance.

At present, the most commonly used aging cost models for BESS optimal operation are power-oriented and energy-oriented approaches. In [1], a fixed aging cost is assigned to the charging and discharging power. In [2], the authors found that high-power charging and discharging accelerate battery aging. Some studies further model aging cost as a piecewise function of power [3] or as a quadratic function of power [4]. Other works assume a linear relationship between aging cost and energy throughput [5]–[6]. However, studies have shown that BESS aging primarily occurs during complete charge–discharge cycles, with the cycle depth being the key factor influencing the aging rate [7]. Thus, power- or energy-based models deviate from the aging mechanism of batteries.

This work was supported by The National Natural Science Foundation of China (U22B20110, 52207098)

Jiaxiong Xiang, Ming Zhou, Zhaoyuan Wu and Zhi Zhang are with the State Key Laboratory of Alternate Electrical Power System with Renewable Energy Sources, School of Electrical  Electronic Engineering, North China Electric Power University, 102206, Beijing, China. (Email: zhouming@ncepu.edu.cn).

In practice, BESS often experience alternating shallow and deep cycles, with complete cycles forming across multiple time periods. Operations in one period affect subsequent marginal aging costs, indicating temporal coupling in BESS aging. Currently, cycle identification commonly relies on the rainflow counting method, which can extract complete cycles from SoC trajectories and has been widely adopted in international standards. However, the rainflow counting method is a post-processing statistical tool based on simulation results and does not possess a closed-form analytical expression. It can only be applied offline when the SoC trajectory is known, making it unsuitable for direct integration into optimization models where SoC is a decision variable.

To address this limitation, existing cycle-based aging cost models often adopt simplified representations. Some studies regard single-period charge or discharge as a cycle [8], while others define aging by single-period discharge depth [9]. These approaches overlook cross-period cycle formation, causing aging costs to be underestimated. In [9], equivalent simplified cycles are defined by identifying consecutive charging and discharging periods, but this approach introduces nonlinear constraints that increase computational complexity. In [10], the BESS is divided into multiple sub-units according to the aging function to represent marginal costs at different depths, but aging is considered only during discharge, which is inconsistent with the actual physical mechanism. These models incorporate simplified cycle-based aging costs into optimization frameworks; however, the aging estimated during optimization often deviates significantly from the actual operating cost, hindering the BESS from achieving optimal economic performance.

Other studies adopt machine learning–based methods for aging-aware BESS scheduling. In [12], a neural network estimator is designed to predict aging cost based on the SoC difference between adjacent periods. In [13], the rainflow counting–based cycle information is encoded into the reward function. However, such data-driven methods require large amounts of training data and often fail to guarantee global optimality in decision-making.

In summary, existing power- and energy-based models fail to capture the cycle depth-dependent nature of battery aging. While cycle-based models better reflect physical aging, accurate cycle identification methods like rainflow counting

979-8-3315-8138-1

lack analytical form and cannot be integrated into optimization frameworks. Simplified alternatives often miss partial cycles and underestimate aging costs. Therefore, a model that accurately captures cycle aging and supports multi-period optimization is urgently needed to improve BESS performance.

This paper conducts innovative research to address the above challenges and develops a dual energy distribution–based cycle aging cost model for BESS. The main contributions are as follows:

(1) A virtual slot framework is introduced, dividing the BESS into multiple slots. The dual energy distribution in these virtual slots captures the marginal deepening effects of charging and discharging cycles, thereby restoring the Markov property of battery aging and enabling state-based aging cost evaluation without dependence on historical SoC or simulations.

(2) Building on this Markovian aging representation, a cycle-oriented aging cost model is developed. By assigning distinct aging costs to virtual slots and imposing corresponding power–energy constraints, the model enables a linearized integration of aging cost into optimization frameworks such as BESS arbitrage or power system operation, ensuring both accurate aging characterization and computational efficiency.

(3) The proposed model delivers over 17.8% higher average arbitrage profit than conventional aging models. It reduces the cost estimation error from over 44% to nearly zero. When integrated into system scheduling, the model further reduces operating costs.

## II. Markov Property Restoration in BESS aging

This section introduces the mechanism of BESS cycle aging and its temporal coupling. By expanding the state with energy distribution variables, the SoC trajectory-dependent aging process is reformulated into a state-based representation, restoring the Markov property and enabling linear modeling.

### A. Battery cycle aging characteristics

The aging caused by cycling can be characterized by a cycle-depth function:

$$Q_{\text{cyc}}(k, d) = kad^{z} \tag{1}$$

where $d$ is the cycle depth, $k$ the cycle type ($k = 1$ for a full cycle and $k = 0.5$ for a half cycle), and $a$ and $z$ are constants determined by battery materials. The aging cost is allocated according to the battery replacement cost $C^{\text{rep}}$:

$$c(k, d) = C^{\text{rep}} Q_{\text{cyc}}(k, d) \tag{2}$$

The rainflow counting is a standard approach for cycle identification, incorporated into international standards and widely regarded as the benchmark for cycle counting. It simulates a "rainflow" process to identify cycles but lacks a closed-form analytical expression, being defined algorithmically as follows:

$$(\boldsymbol{d}^{\text{full}}, \boldsymbol{d}^{\text{dis}}, \boldsymbol{d}^{\text{ch}}) = \text{rainflow}(\text{SoC}_0, \ldots, \text{SoC}_t) \tag{3}$$

where $\boldsymbol{d}^{\text{full}}$, $\boldsymbol{d}^{\text{dis}}$, and $\boldsymbol{d}^{\text{ch}}$ denote the sets of full cycles, discharge half cycles, and charge half cycles, respectively. Figure 1 illustrates the process of rainflow cycle identification, with detailed rules available in [7].

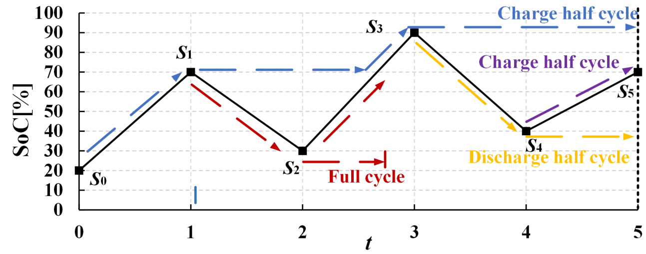


Fig. 1. Rainflow counting cycle recognition.

Cycle-based aging causes the battery aging cost to exhibit temporal coupling, as the operating cost in each period depends on the historical SoC trajectory. However, the rainflow counting method is a post-simulation approach that requires a known SoC trajectory and therefore cannot be embedded into an optimization model where SoC is a decision variable. Hence, a cycle-oriented cost model is required to explicitly quantify the effect of different operational actions on cycle evolution and battery aging.

### B. Markovian Representation of Battery aging

When the SoC changes from $\text{SoC}_t$ to $\text{SoC}_{t+1}$, the transition path $\text{SoC}_t - \text{SoC}_{t+1}$ may intersect with the "raindrops" falling from the historical SoC trajectory. These intercepted raindrops continue to flow along the new trajectory, indicating that the corresponding half cycles are further deepened. In Fig. 1, taking $S_5$ as an example where SoC = 0.7, if discharging starts from $S_5$ and the SoC remains above $0.4$ after discharging, only the half cycle starting at $S_5$ is deepened. When the SoC decreases below $0.4$, the $S_3$–$S_4$ half cycle with a depth of $0.5$ is deepened. Conversely, during charging, the $S_4$–$S_5$ half cycle with a depth of $0.3$ is first deepened; when the SoC exceeds $0.9$, the $S_0$–$S_1$–$S_3$ half cycle with a depth of $0.9$ becomes active and is subsequently deepened.

Figure 2 illustrates the marginal deepening effects on existing half cycles when the BESS charges from $S_5$ to SoC = 1 and discharges to SoC = 0. The solid regions represent the existing half cycles, while the grid-marked regions indicate the additional depths that can be further extended through subsequent charging and discharging operations.

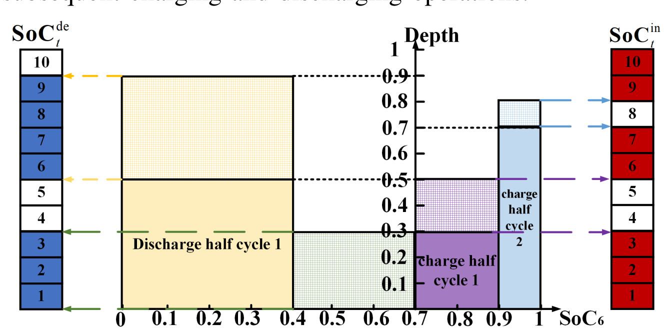


Fig. 2. Impact of charging/discharging and dual energy distribution at S5.

The proposed model introduces energy distribution states based on virtual slots to store and explicitly represent the marginal effects of real-time charging and discharging operations. The BESS is uniformly divided into $I$ virtual slots, each with a maximum state of charge of $1/I$, and indexed by depth from shallow to deep as $i = 1, \ldots, I$. A virtual slot changing

979-8-3315-8138-1

from full to empty (or vice versa) represents the deepening of a discharge (or charge) half-cycle from $(i-1)/I$ to $i/I$.

Two energy distribution states are defined to describe how discharging and charging affect existing half cycles:

$$\mathbf{SoC}_t^{\mathrm{de}} = [\mathrm{SoC}_{t,1}^{\mathrm{de}}, \ldots, \mathrm{SoC}_{t,i}^{\mathrm{de}}, \ldots, \mathrm{SoC}_{t,I}^{\mathrm{de}}] \tag{4}$$

$$\mathbf{SoC}_t^{\mathrm{in}} = [\mathrm{SoC}_{t,1}^{\mathrm{in}}, \ldots, \mathrm{SoC}_{t,i}^{\mathrm{in}}, \ldots, \mathrm{SoC}_{t,I}^{\mathrm{in}}] \tag{5}$$

where $\mathrm{SoC}_t^{\mathrm{de}}$ denotes the energy distribution for discharge aging, with energy allocated to slots representing the marginal deepening of discharge half cycles; and $\mathrm{SoC}_t^{\mathrm{in}}$ denotes the energy distribution for charging, with energy vacancies corresponding to the marginal deepening of charge half cycles. $\mathrm{SoC}_{t,i}^{\mathrm{de}}$ and $\mathrm{SoC}_{t,i}^{\mathrm{in}}$ denote the energy state of slot $i$ at time $t$. Figure 2 illustrates the energy distributions of $\mathrm{SoC}_{i,t}^{\mathrm{de}}$ (blue) and $\mathrm{SoC}_{i,t}^{\mathrm{in}}$ (red) at state $S_5$, where white cells indicate empty slots and the numbers denote the virtual slot indices. Fig. 3 presents the corresponding dual energy distributions at different time instants.

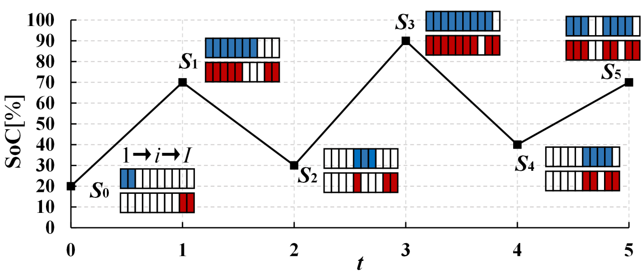


Fig. 3. Dual Energy Distribution Representation.

At any given time, the impact of future operations at any depth on historical cycles or incremental aging cost can be determined from the energy distribution of virtual slots:

$$c_t = g\left(\mathbf{SoC}_t^{\mathrm{de}}, \mathbf{SoC}_t^{\mathrm{in}}, \Delta\mathrm{SoC}_t\right) \tag{6}$$

An action-based mechanism updates $\mathbf{SoC}_t^{\mathrm{de}}$ and $\mathbf{SoC}_t^{\mathrm{in}}$ to restore the Markov property:

$$\mathbf{SoC}_{t+1}^{\mathrm{de}}, \mathbf{SoC}_{t+1}^{\mathrm{in}} = f\left(\mathbf{SoC}_t^{\mathrm{de}}, \mathbf{SoC}_t^{\mathrm{in}}, \Delta\mathrm{SoC}_t\right) \tag{7}$$

The unified state update rule for $\mathbf{SoC}_t^{\mathrm{de}}$ and $\mathbf{SoC}_t^{\mathrm{in}}$ can be expressed as follows: During charging, energy is sequentially filled into the unoccupied virtual slots from $i=1$ to $I$, while during discharging, energy is sequentially released from the virtual slots in the same order. The energy distribution shown in Fig. 3 further validate this transition rule, expressed as:

$$\Delta\mathrm{SoC}_t = \sum_{i\in\mathcal{I}} \Delta\mathrm{SoC}_{i,t}^{x}, \quad x \in \{\mathrm{in}, \mathrm{de}\} \tag{8}$$

$$\Delta\mathrm{SoC}_{i,t}^{x} > 0 \text{ if } \mathrm{SoC}_{j,t}^{x} = \tfrac{1}{I},\ \forall j < i \text{ and } \Delta\mathrm{SoC}_t > 0 \tag{9}$$

$$\Delta\mathrm{SoC}_{i,t}^{x} < 0 \text{ if } \mathrm{SoC}_{j,t}^{x} = 0,\ \forall j < i \text{ and } \Delta\mathrm{SoC}_t < 0 \tag{10}$$

This update process effectively realizes the pairing of charge and discharge half-cycles into full cycles and removes the paired-cycle from the energy distribution.

When the capacity of each virtual slot matches the minimum inter-temporal SoC variation of the BESS (For example, if the BESS operates with a charge/discharge step size of $\Delta\mathrm{SoC} = 0.1$, it can be divided into $I = 10$ virtual slots, each having a maximum SoC of $1/I = 0.1$. ), the aging cost calculated by the proposed method is strictly equivalent to the ex-post results of the rainflow counting method.

By representing the deepening of cycles through energy distribution states, this approach restores the Markov property of cycle aging. Meanwhile, the state updating process eliminates the nonlinear comparison of extrema required in traditional rainflow counting, offering the potential for linear modeling and seamless integration into optimization frameworks.

## III. BESS Aging Cost Model Based on Dual Energy Distribution

After restoring the Markov property, this section formulates aging constraints and cost, enabling a linear model suitable for optimization tasks like BESS arbitrage and system operation.

### A. Aging Cost Model

The aging cost model incorporates the following constraints: the energy distribution constraint, the total energy balance and boundary constraints of virtual slots, the virtual slot power constraint, and the virtual slot energy transition constraint.

(1) Initial Energy Distribution Constraint

When the initial SoC is $\mathrm{SoC}_0$, in the energy distribution state $\mathbf{SoC}_t^{\mathrm{de}}$, energy is sequentially filled from the lowest slot index ($i=1$) to higher ones. In contrast, in the energy distribution state $\mathbf{SoC}_t^{\mathrm{in}}$, energy is filled from the highest slot index ($i=I$) down to lower ones:

$$\mathrm{SoC}_{0,i}^{\mathrm{de}} = \frac{1}{I}\mathbf{1}_{\left\{\frac{i}{I} \le \mathrm{SoC}_0\right\}} \tag{11}$$

$$\mathrm{SoC}_{0,i}^{\mathrm{in}} = \frac{1}{I}\mathbf{1}_{\left\{\frac{i}{I} \ge \mathrm{SoC}_0\right\}} \tag{12}$$

where, $\mathbf{1}_{\{\cdot\}}$ equals 1 when the condition inside the brackets is satisfied and 0 otherwise. Such an initial energy distribution ensures that, regardless of charging or discharging operations, each half cycle deepens progressively from zero depth.

(2) The total energy of the two types of energy distributions should be equal to the total energy of the BESS.

$$\sum_{i\in I} \mathrm{SoC}_{t,i}^{\mathrm{de}} = \sum_{i\in I} \mathrm{SoC}_{t,i}^{\mathrm{in}} = \mathrm{SoC}_t \tag{13}$$

(3) The energy constraints of the virtual slots:

$$0 \le \mathrm{SoC}_{t,i}^{\mathrm{de}} \le \frac{1}{I} \tag{14}$$

$$0 \le \mathrm{SoC}_{t,i}^{\mathrm{in}} \le \frac{1}{I} \tag{15}$$

(4) Assign the charging and discharging power separately to the two types of energy distributions, ensuring that the total power in each distribution equals the actual charging or discharging power of BESS.

$$\sum_{i\in I} P_{t,i}^{\mathrm{de,c}} = \sum_{i\in I} P_{t,i}^{\mathrm{in,c}} = P_t^{\mathrm{c}} \tag{16}$$

$$\sum_{i\in I} P_{t,i}^{\mathrm{de,d}} = \sum_{i\in I} P_{t,i}^{\mathrm{in,d}} = P_t^{\mathrm{d}} \tag{17}$$

where $P_t^{\mathrm{c}}$ and $P_t^{\mathrm{d}}$ denote the charging and discharging power of the BESS, respectively; $P_{t,i}^{\mathrm{de,c}}$ and $P_{t,i}^{\mathrm{de,d}}$ represent the charging and discharging power of virtual slot $i$ in the energy distribution state $\mathbf{SoC}_t^{\mathrm{de}}$; and $P_{t,i}^{\mathrm{in,c}}$ and $P_{t,i}^{\mathrm{in,d}}$ denote the

979-8-3315-8138-1

charging and discharging power of virtual slot $i$ in the energy distribution state $\mathbf{SoC}_t^{\text{in}}$.

(5) Energy transition constraints for virtual slots:

$$\text{SoC}_{t,i}^{\text{de}} = \text{SoC}_{t-1,i}^{\text{de}} + \frac{\eta P_{t,i}^{\text{de,c}} \Delta t}{E_{\max}} - \frac{P_{t,i}^{\text{de,d}} \Delta t}{\eta E_{\max}} \tag{18}$$

$$\text{SoC}_{t,i}^{\text{in}} = \text{SoC}_{t-1,i}^{\text{in}} + \frac{\eta P_{t,i}^{\text{in,c}} \Delta t}{E_{\max}} - \frac{P_{t,i}^{\text{in,d}} \Delta t}{\eta E_{\max}} \tag{19}$$

where $\eta$ denotes the efficiency of the BESS.

The unit aging cost for each virtual slot $c_i$ (\$/MWh) is obtained by normalizing the aging increment of a charge or discharge half cycle by the slot capacity and multiplying by the battery replacement cost.

$$c_i = C^{\text{rep}} \frac{Q_{\text{cyc}}\left(\frac{1}{2}, d\right) - Q_{\text{cyc}}\left(\frac{1}{2}, d-1\right)}{E_{\max}/I} \tag{20}$$

The aging cost of the BESS at each time step is equal to the sum of the aging costs of all virtual slots. Specifically, the discharging aging cost is calculated based on the energy distribution state $\mathbf{SoC}_t^{\text{de}}$, while the charging aging cost is obtained from the energy distribution state $\mathbf{SoC}_t^{\text{in}}$.

$$C_t = \sum_{i \in I} \frac{c_i}{2E_{\max}} \left( \frac{P_{t,i}^{\text{de,d}} \Delta t}{\eta} + \eta P_{t,i}^{\text{in,c}} \Delta t \right) \tag{21}$$

By assigning progressively increasing unit aging costs $c_i$ to each virtual slot, the state transition rule of filling and extracting energy in the fixed order $i = 1 \to I$ is automatically satisfied within the optimization problem.

### B. BESS Operation Model

The proposed model, together with the BESS power constraints and energy upper and lower bounds, constitutes a complete operational model of BESS:

$$0 \le P_t^{\text{d}} \le \lambda_t^{\text{d}} P^{\max}, \tag{22}$$

$$0 \le P_t^{\text{c}} \le \lambda_t^{\text{c}} P^{\max}, \tag{23}$$

$$\lambda_t^{\text{d}} + \lambda_t^{\text{c}} = 1, \quad \lambda_t^{\text{d}}, \lambda_t^{\text{c}} \in \{0, 1\}, \tag{24}$$

$$\text{SoC}^{\min} \le \text{SoC}_t \le \text{SoC}^{\max}. \tag{25}$$

Cost-related constraints (11)–(21)

where $\lambda_t^{\text{d}}$ and $\lambda_t^{\text{c}}$ are the discharge and charge state variables of the BESS, respectively. The BESS energy transfer is managed by tracking each virtual slot, removing the need to monitor total energy. This model can be seamlessly and linearly integrated into optimization frameworks like energy arbitrage and power system operation.

## IV. CASE STUDY

This section presents a case study to validate the proposed cost model and compare it with traditional ones, evaluating its effectiveness in improving BESS arbitrage profits and reducing overall system operating costs.

### A. Parameter Settings

The BESS, rated at 600 MW/2400 MWh, is analyzed under two scenarios: (1) standalone energy arbitrage using the PJM market price curve from [15], and (2) integrated operation within the IEEE 118-bus system to assess its impact on overall grid optimization. The battery replacement cost $C_{\text{rep}}$ is set to 300,000 \$/MWh, with aging parameters $a = 0.0002$ and $z = 2.03$ [11], and an initial state of charge $\text{SoC}_0 = 0.8$. All simulations are performed on a computer equipped with an Intel i7–14700K CPU and 32 GB of RAM.

To further investigate the impact of the proposed cost model on market clearing performance, five different cost models are designed and compared.

TABLE I
COMPARATIVE EXAMPLE

| Case | Aging Cost Model Description |
|---|---|
| 1 | Fixed aging cost assigned to charge/discharge power [1]. |
| 2 | Single-period charging or discharging is treated as one cycle with a piecewise cost function of cycle depth [10]. |
| 3 | Fixed aging cost applied to discharged energy only [5]. |
| 4 | Aging concentrated on discharge; the BESS is modeled as multiple sub-systems with different aging costs [11]. |
| 5 | The proposed aging cost model, with $I = 20$. |

### B. Comparison of BESS Arbitrage Profits

Different cost models are embedded in the arbitrage framework for comparison, and Fig. 4 shows that they yield markedly different SoC trajectories. To evaluate the accuracy of the cost model, the aging cost calculated in the decision-making stage is defined as the *calculated cost*, while the result obtained by applying the rainflow counting method to the actual SoC trajectory is regarded as the *actual cost*. The relative cost error is defined as $\varepsilon = \frac{|\text{Calculated Cost} - \text{Actual Cost}|}{\text{Actual Cost}}$. Figure 5 presents a comparison among five cost models. The results show that the absolute error of traditional models ranges from 44% to 62%, whereas the proposed model achieves a deviation of only 0.01%. By subtracting the actual aging cost from the market arbitrage revenue, the actual profit of the BESS is obtained, as shown in Figure 5. The results indicate that the proposed aging cost model achieves the highest arbitrage profit, improving by \$8077 (about 17%) over the second-best model. We conducted a sensitivity analysis on the number of virtual slots in Model 5. The results show that the arbitrage profit saturates at around 10 slots, while the computation time remains negligible even with 50 slots (0.0098 s).

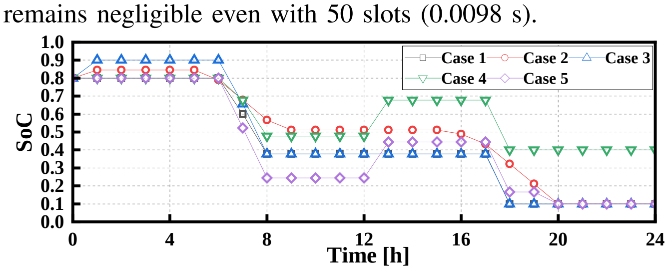


Fig. 4. SoC trajectories in different cases.

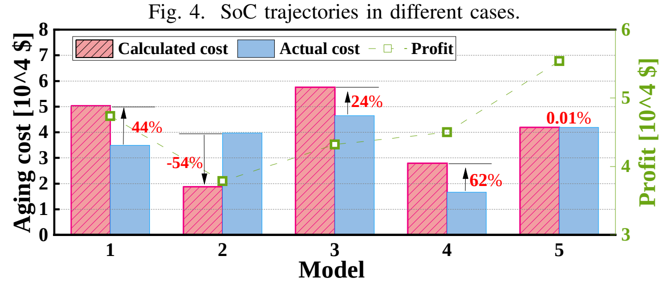


Fig. 5. Cost calculation error and profit comparison across different cases

979-8-3315-8138-1

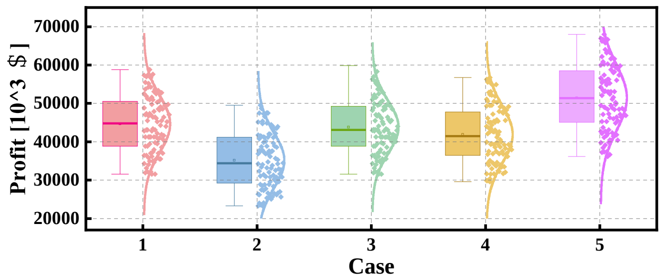

Fig. 6. BESS Profit comparison in different cases.

To evaluate the proposed model's arbitrage performance under varying price scenarios, 100 days of PJM market data were simulated. As shown in Figure 6, the model yields the highest average profit of \$51,477—about 13%–31% higher than other models.

### C. Comparison of System Operating Costs

The cost model of the BESS is incorporated into the scheduling optimization of the IEEE 118-bus system. Based on the fuel costs of thermal units and the actual aging costs of the BESS, the total system operating cost is obtained, as illustrated in Fig. 7. The results show that the proposed model achieves the lowest system cost, reducing total expenses by \$4,000–\$7,000 compared with other cases. Meanwhile, the computation time remains below 1 s, demonstrating that the proposed linearized aging cost model attains high accuracy while maintaining excellent computational efficiency.

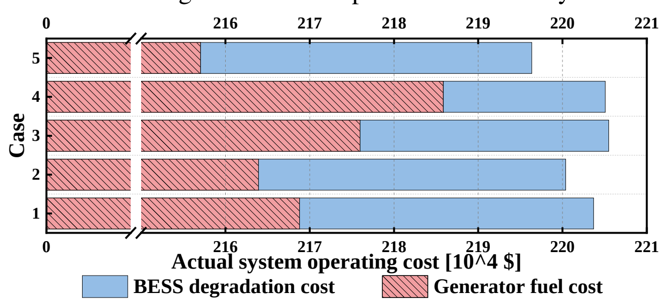

Fig. 7. Comparison of System Operating Costs.

## CONCLUSIONS

The aging that occurs in the charging and discharging cycles of BESS has a significant impact on its operational benefits. Cycle identification usually relies on rainflow counting for post hoc SoC analysis, but analytical and accurate cycle cost models are lacking in optimization problem. To address this, this paper proposes a dual energy distribution state model that accurately characterizes cycle aging costs.

A virtual slot framework is introduced, dividing the BESS into multiple slots. The dual energy distribution across these virtual slots captures the marginal deepening effects of charging and discharging cycles, thereby restoring the Markov property of battery aging. Based on this, a cycle-dependent linear aging cost model is developed, transforming the traditional nonlinear, history-dependent aging process into a state-based linear analytical model that can be seamlessly embedded into the optimization framework.

Case studies show that the proposed model improves the average arbitrage profit by more than 17% compared with conventional aging models. Traditional methods produce over 44% cost estimation errors during optimization, while the aging cost computed by the proposed model deviates from the benchmark rainflow counting result by only 0.01%. When integrated into the power system scheduling model, the proposed method further reduces the total system operating cost, demonstrating its effectiveness in both economic optimization and grid-level operation.

With its high accuracy and linear, binary-free formulation, the proposed method is broadly applicable to battery technologies with convex degradation functions (e.g., lithium-ion, lead–acid, and nickel–cadmium). It can be incorporated as an additional constraint into a wide range of BESS optimization problems (including joint energy and ancillary-service co-optimization) and market-clearing models with marginal pricing, enabling cost-accurate bidding and market mechanism design as well as broader BESS operation studies.

## REFERENCES


[1] S. Bhattacharjee and R. Sioshansi, "Comparing Participation Models in Electricity Markets for Hybrid Energy-Storage Resources," *IEEE Trans. Power Syst.*, vol. 40, no. 1, pp. 650–661, Jan. 2025.

[2] O. N. Omar *et al.*, "Lithium iron phosphate based battery – Assessment of the aging parameters and development of cycle life model," *Appl. Energy*, vol. 113, pp. 1575–1585, Jan. 2014.

[3] X. Fang, H. Guo, and X. Zhang, "An efficient and incentive-compatible market design for energy storage participation," *Appl. Energy*, vol. 311, p. 118731, Apr. 2022.

[4] X. Tan, G. Qu, B. Sun, and N. Li, "Optimal Scheduling of Battery Charging Station Serving Electric Vehicles Based on Battery Swapping," *IEEE Trans. Smart Grid*, vol. 10, no. 2, pp. 1372–1384, Mar. 2019.

[5] F. Sorourifar, V. M. Zavala, and A. W. Dowling, "Integrated Multiscale Design, Market Participation, and Replacement Strategies for Battery Energy Storage Systems," *IEEE Trans. Sustain. Energy*, vol. 11, no. 1, pp. 84–92, Jan. 2020.

[6] K. Antoniadou-Plytaria, D. Steen, L. A. Tuan, "Market-based energy management model of a building microgrid considering battery aging," *IEEE Trans. Smart Grid*, vol. 12, no. 2, pp. 1794–1804, Mar. 2021.

[7] B. Xu, A. Oudalov, A. Ulbig, G. Andersson, and D. S. Kirschen, "Modeling of lithium-ion battery aging for cell life assessment," *IEEE Trans. Smart Grid*, vol. 9, no. 2, pp. 1131–1140, Mar. 2018.

[8] M. Chen, Z. Liang, and Z. Cheng, "Optimal Scheduling of FTPSS With PV and HESS Considering the Online Degradation of Battery Capacity," *IEEE Trans. Transp. Electrif.*, vol. 8, no. 1, pp. 936–947, Mar. 2022.

[9] S. Fang, B. Gou, Y. Wang, Y. Xu, C. Shang, and H. Wang, "Optimal Hierarchical Management of Shipboard Multibattery Energy Storage System Using a Data-Driven Aging Model," *IEEE Trans. Transp. Electrif.*, vol. 5, no. 4, pp. 1306–1318, Dec. 2019.

[10] C. Ju, P. Wang, and L. Goel, "A Two-Layer Energy Management System for Microgrids With Hybrid Energy Storage Considering Aging Costs," *IEEE Trans. Smart Grid*, vol. 9, no. 6, pp. 6047–6057, Nov. 2018.

[11] B. Xu, J. Zhao, T. Zheng, and E. Litvinov, "Factoring the Cycle Aging Cost of Batteries Participating in Electricity Markets," *IEEE Trans. Power Syst.*, vol. 33, no. 2, pp. 2248–2259, Mar. 2018.

[12] X. Zhao and X. Li, "Microgrid Optimal Energy Scheduling Considering Neural Network Based Battery Aging," *IEEE Trans. Power Syst.*, vol. 39, no. 1, pp. 1594–1606, Jan. 2024.

[13] K.-B. Kwon and H. Zhu, "Reinforcement Learning-Based Optimal Battery Control Under Cycle-Based Aging Cost," *IEEE Trans. Smart Grid*, vol. 13, no. 6, pp. 4909–4917, Nov. 2022.

[14] Z. Liu, X. Wang, and K. Yang, "Analytical Model of Rainflow-Based Cyclic Aging for Economic Battery Dispatch Optimization," *IEEE Trans. Energy Convers.*, vol. 39, no. 4, pp. 2425–2438, Dec. 2024.

[15] Q. Ma, W. Wei, and S. Mei, "A Two-Timescale Operation Strategy for Battery Storage in Joint Frequency and Energy Markets," *IEEE Trans. Energy Markets, Policy and Regulation*, vol. 2, no. 2, pp. 200–213, Jun. 2024.


979-8-3315-8138-1